Efficient and Stable Perovskite White Light-Emitting Diodes for Backlit Display

Shuxin Chen, Jidong Lin, Song Zheng, Yuanhui Zheng, and Daqin Chen*

High-quality backlit display puts forward urgent demand for color-converting materials. Recently, metal halide perovskites (MHPs) with full spectral tunability, high photoluminescence quantum yields (PLQYs), and high color purity have found potential application in wide-color-gamut display. Regrettably, naked MHPs suffer from long-term instable issue and cannot pass harsh stability tests. Herein, amorphous-glass-protected green/red $CsPbX_3$ quantum dots (QDs) are prepared by elaborately optimizing glass structure, perovskite concentration, and in situ crystallization. PLQYs of green $CsPbBr_3$@glass and red $CsPbBr_{1.5}I_{1.5}$@glass reach 94% and 78%, respectively, which are the highest ones of $CsPbX_3$@glass composites reported so far and comparable to colloidal counterparts. Benefited from complete isolation of QDs from external environment by glass network, $CsPbX_3$@glass can endure harsh commercial standard aging tests of 85 °C/85%RH and blue-light-irradiation, which are applied to construct white light-emitting diodes (wLEDs) with high external quantum efficiency of 13.8% and ultra-high luminance of 500 000 cd m^{-2}. Accordingly, the perovskite wLED arrays-based backlit unit and a prototype display device are designed for the first time, showing more vivid and wide-color-gamut feature benefited from narrowband emissions of $CsPbX_3$ QDs. This work highlights practical application of $CsPbX_3$@glass composite as an efficient and stable light color converter in backlit display.

1. Introduction

QDs are a unique type of emitters with size-tunable emissions, high color purity, PLQY, and excellent solution processability.[1] The well-developed CdSe-based QDs have been commercially used as light-conversion materials (LCMs) for back-lighting in liquid-crystal displays (LCDs) to improve color gamut, leading to the booming of QD televisions in market.[2,3] For example, the color gamut of LCD using conventional phosphors as LCM is ≈72% of National Television System Committee (NTSC) standard, which can be improved to ≈110% of NTSC standard after utilizing QD-LCM.[4] However, the widely used CdSe-based QDs have been widely limited by many countries for the presence of toxic heavy metal cadmium element. Therefore, searching non-Cd QDs for wide-color-gamut LCD is highly demanded.

As one of the hottest optoelectronic materials, MHPs have been proven to be excellent light emitters, and attracted attention for their potential in electroluminescent (EL) LEDs.[5,6] By engineering their structure and composition, MHPs show the ability of full spectral tunability in the visible region,[7] ≈100% PLQY,[8–10] and ultra-narrow full width at half maximum (fwhm, down to 12 nm).[11] In the past few years, perovskite LED efficiency has enhanced in external quantum efficiency (EQE) from 0.0125% to >20% (blue: 14.82%, green: 28.9%, red: 25.8%, white: 12.2%).[12–16] Notably, the EL-LEDs (self-emissive devices using the current-driving mode) are used for active-matrix displays rather than back-lighting LCDs, which has still a long-way to go for the commercialization of this exciting technology. On the contrary, the phosphors-converted PL-LEDs have been well developed, and the commercial backlit unit in LCDs consisting of InGaN blue chip and conventional phosphors, such as $Y_3Al_5O_{12}$: Ce (YAG: Ce), β-SiAlON: Eu^{2+}, and K_2SiF_6: Mn^{4+}.[17–21] Therefore, the replacement of conventional phosphors by MHPs to construct wLEDs as back-lighting unit used in LCD is an effective way to enlarge color gamut and has promising commercial application.[22]

Regrettably, naked MHPs suffers from long-term instable issue, which cannot pass harsh stability tests, especially the commercial standards of 85°C/85% RH stability and blue–light-irradiation stability. Among several reported strategies,[23–31]

S. Chen, J. Lin, S. Zheng, D. Chen
College of Physics and Energy
Fujian Normal University
Fuzhou, Fujian 350117, P. R. China
E-mail: dqchen@fjnu.edu.cn
S. Chen, Y. Zheng, D. Chen
Fujian Science & Technology Innovation Laboratory for Optoelectronic Information
Fuzhou, Fujian 350116, P. R. China
Y. Zheng
College of Chemistry
Fuzhou University
Fuzhou, Fujian 350116, P. R. China
D. Chen
Fujian Provincial Collaborative Innovation Center for Advanced High-Field Superconducting Materials and Engineering
Fuzhou, Fujian 350117, P. R. China
D. Chen
Fujian Provincial Engineering Technology Research Center of Solar Energy Conversion and Energy Storage
Fuzhou, Fujian 350117, P. R. China

embedding MHPs inside robust inorganic glass is believed to be feasible for the effective isolation of MHPs from external environment. To date, all-inorganic $CsPbX_3$ (X = Cl, Br, and I) perovskite QDs (PeQDs) have been successfully precipitated in a variety of glasses via in situ nucleation/growth.[32–39] However, unlike wet-chemical synthesis, the dense glass network structure will hinder the diffusion of Cs^+, Pb^{2+}, and X^- ions, and impede $CsPbX_3$ nanocrystallization inside glass, which makes PLQYs of $CsPbX_3$@glass lower than those of colloidal counterparts. Herein, we have successfully optimized SiO_2-B_2O_3-ZnO-CaF_2 glass network, perovskite component concentrations, and glass crystallization conditions to fabricate high-quality $CsPbX_3$@glass. PLQYs of green $CsPbBr_3$@glass and red $CsPbBr_{1.5}I_{1.5}$@glass can reach as high as 93.8% and 78.1%, respectively, which are the highest values for $CsPbX_3$@glass composites as far as we know (Tables S1 and S2, Supporting Information). Importantly, the $CsPbX_3$@glass exhibits excellent long-term stability, and satisfies commercial standards of 85°C/85% RH and blue-light-irradiation stability. As an application demo, a high-brightness wLED with EQE of 13.84% and luminance of 500 000 cd m^{-2} is designed and applied in back-lighting module to realize wide-color-gamut display with 127% of NTSC standard.

2. Result and Discussion

The glass network structure, appropriate concentration of perovskite components and heat-treatment condition will play key roles in improving optical performance of $CsPbX_3$@glass. We use a well-designed SiO_2–B_2O_3–ZnO–CaF_2 glass as the host to investigate the effect of perovskite concentrations (Cs_2CO_3–PbX_2–NaX, X = Br, I) and heat-treatments on optical properties of in situ grown $CsPbX_3$ (Tables S3–S6, Supporting Information). The presence of these elements in the glass is confirmed by energy dispersive X-ray (EDX) and X-ray photoelectron spectroscopy (XPS) data (Figures S1 and S2, Supporting Information). As illustrated in **Figure 1**a, for the borosilicate glass, $[BO_4]^-$ tetrahedra will partially replace $[SiO_4]$ ones in the silicate network, and charge imbalance is compensated by network modifying Zn^{2+} ions.[40,41] High-content B_2O_3 will lead to increase of $[BO_3]$ triangular unit, which is conducive to the formation of a 2D glass network, and the introduced CaF_2 can release F^- ions, which can break inherent bridging oxygen bond (Si—O) and form lots of non-bridging oxygen.[42,43] Consequently, the present glass network can provide sufficient passages and spaces for Cs^+, Pb^{2+}, and Br^- diffusion and promote nucleation/growth of $CsPbX_3$.

Fourier transform infrared (FTIR) spectrum proves the presence of vibrational structures of Si—O and B—O in the glass. As depicted in Figure 1b, a weaker band at 650–750 cm^{-1} is designated to binding vibration of B—O—B group in the borate segment. B—O stretching vibration in the $[BO_3]$ triangle is located at 1300–1550 cm^{-1}, while the absorption band at 1000–1100 cm^{-1} belongs to bending vibration of Si—O—Si bond in the $[SiO_4]$ tetrahedral unit as well as stretching vibration of the $[BO_4]$ unit.[44–46] As evidenced in Figure 1c,d, ^{11}B magic-angle spinning (MAS) nuclear magnetic resonance (NMR) spectrum confirms the existence of $[BO_3]$ (−3 ppm) and $[BO_4]$ (9 ppm) units,

and ^{19}F NMR spectrum supports the formation of Si—F bond (−142 ppm) in the glass network.[47,48] X-ray diffraction (XRD) patterns evidence the precipitation of $CsPbX_3$ (X_3 = Br_3, $Br_{1.5}I_{1.5}$) inside glass. As shown in Figure 1e, the precursor glass (PG) shows a typical amorphous structure, and typical cubic $CsPbX_3$ crystalline diffraction peaks are superimposed on the amorphous halo after heat treatment. High-angle annular dark-field (HAADF) scanning transmission electron microscope (STEM) image (inset of Figure 1f) and high-resolution TEM (HRTEM) micrograph (Figure 1f) confirm homogenous distribution of $CsPbX_3$ PeQDs with high crystallinity and sizes of 5–10 nm among glass matrix.

As shown in **Figure 2**a, $CsPbBr_3$@glass samples with various perovskite concentrations exhibit tunable cyan-green emissions (509–524 nm) under 450 nm blue light excitation. PL peak and absorption shoulder gradually red-shift (Figure 2a; Figure S3a, Supporting Information) and decay lifetime monotonously increases (Figure S3c–f, Supporting Information) with increase of perovskite concentration, indicating that the bandgap energy of the precipitated $CsPbBr_3$ PeQDs can be finely modified by varying perovskite concentration. The fwhm values of $CsPbBr_3$@glass are in the range of 23.3–26.7 nm (Figure 2b), confirming the $CsPbBr_3$@glass exhibits a narrowband PL with high color purity. Meanwhile, PLQY of $CsPbBr_3$@glass shows a tendency of enhancement and then gradually decreases with increase of perovskite concentration. The best PLQY is ≈94% for the sample with perovskite concentration of 0.875 (Figure 2c), which is the highest value reported as far as we know (Table S1, Supporting Information). Increasing perovskite concentration in glass is beneficial for the diffusion of Cs^+, Pb^{2+}, and X^- ions and the promotion of high-crystallinity $CsPbX_3$ growth, leading to the uptrend in PLQY. The decrease in PLQY with further increase of perovskite concentration is probably due to excessive growth of $CsPbBr_3$ PeQDs accompanied with an increase in the number of defects as non-radiative relaxation centers.[49] Similarly, fwhm shows a rapid broadening when perovskite concentration is higher than 0.875, which is attributed to particle inhomogeneity caused by overgrowth of $CsPbBr_3$ PeQDs. Importantly, the same phenomenon is observed for the red-emitting $CsPbBr_{1.5}I_{1.5}$@glass (Figure 2d–f). As the perovskite concentration increases, both the PL peak (625–637 nm) and the absorption shoulder red-shift (Figure 2d; Figure S3b, Supporting Information). The PLQY of $CsPbBr_{1.5}I_{1.5}$@glass is also dependent on perovskite concentration (Figure 2f and Table S2, Supporting Information). When the perovskite concentration exceeds 1.05, the overgrowth of $CsPbBr_{1.5}I_{1.5}$ PeQDs results in a decrease in PLQY and a gradual broadening of fwhm (Figure 2e,f).

Additionally, crystallization condition also plays a crucial role for improving optical properties of $CsPbX_3$@glass samples. Herein, S_{2G}-S_{5G} for $CsPbBr_3$@glass and S_{5R}-S_{7R} for $CsPbBr_{1.5}I_{1.5}$@glass are chosen and are heat-treated at different temperatures of 480, 500, 520, and 540 °C for 2 h. As illustrated in **Figure 3** and Table S5 (Supporting Information), PL spectra of samples S_{2G}-S_{5G} all show a red-shifting and the corresponding fwhms are narrowed with elevation of heat-treatment temperature. Higher temperature heat-treatment can promote migration and diffusion of perovskite ions, thus facilitating more uniform growth of $CsPbBr_3$ PeQDs inside
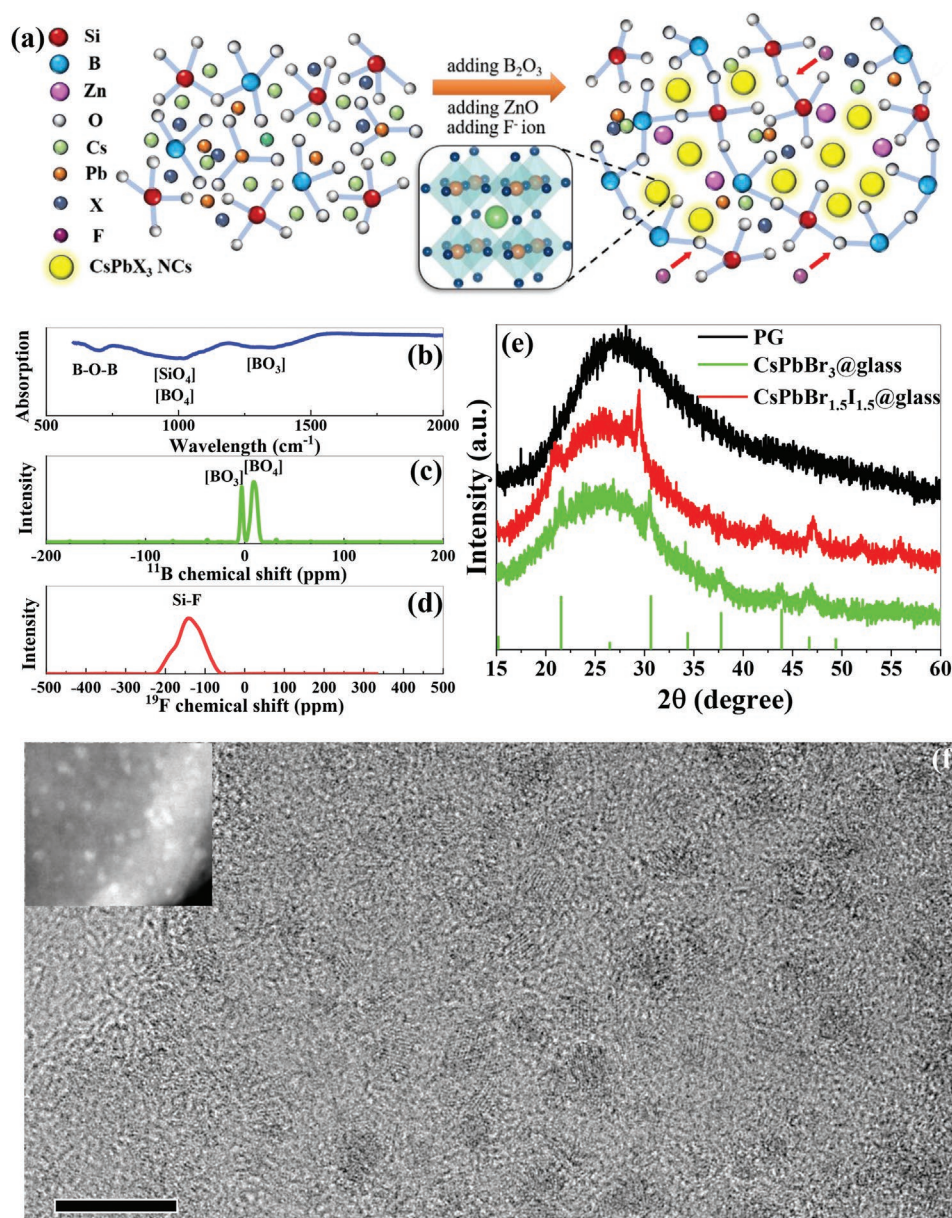
Figure 1. a) Schematic illustration of SiO_2-B_2O_3-ZnO-CaF_2 glass network structure and in-situ growth of $CsPbX_3$ PeQDs. b) FTIR spectrum, c) ^{11}B and d) ^{19}F NMR spectra of the glass. e) XRD patterns of precursor glass and $CsPbX_3$@glass. Bars represent standard diffraction data of cubic $CsPbBr_3$ crystal (JCPDS No. 54-0752). f) A typical HRTEM micrograph and HADDF-STEM image (inset) of $CsPbBr_3$@glass.

glass. However, PLQY of $CsPbBr_3$@glass does not always enhances with elevation of heating temperature (Figures 3f). For example, heat-treatment temperature exceeds the optimal temperature (500°C for S_{4G}), PLQY gradually decreases. Too high crystallization temperature will overgrow $CsPbBr_3$ PesQDs, which leads to increase the number of defects acting as non-radiative loss centers. Similar results are observed for the S_{5R}-S_{7R} samples (Figure S4 and Table S6, Supporting Information), but it is worth noting that S_{5R} achieves ≈78% PLQY at a heating temperature of 590°C, which is the highest value for $CsPb(Br/I)_3$@glass reported to date (Table S2, Supporting Information). To sum up, by elaborately optimize perovskite

concentration and heat-treatment temperature, green $CsPbBr_3$@glass (S_{4G} heat-treated at 500°C per 2 h) with PL wavelength of 517 nm, PLQY of 93.8% and fwhm of 26.5 nm and red $CsPbBr_{1.5}I_{1.5}$@glass (S_{5R} heat-treated at 590°C per 2 h) with PL wavelength of 640 nm, PLQY of 78.1% and fwhm of 36.1 nm are successfully achieved.

Furthermore, both green $CsPbBr_3$@glass and red $CsPbBr_{1.5}I_{1.5}$@glass samples were subjected to a series of stability tests. As presented in **Figure 4**a,b PL intensity of $CsPbX_3$@glass samples decreases with elevation of temperature owing to intrinsic thermal quenching effect of PeQDs. Fortunately, it is worth noting that $CsPbX_3$@glass exhibits
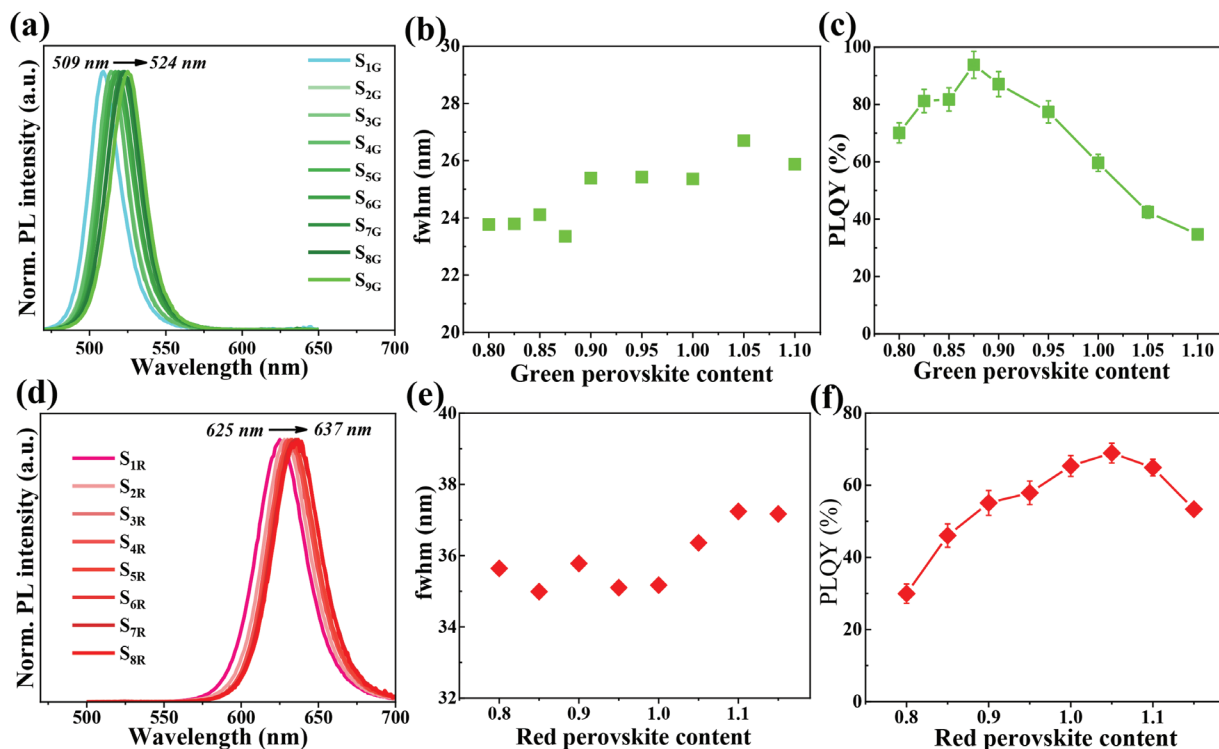
Figure 2. Dependence of PL spectrum, fwhm, and PLQY of a-c) CsPbBr$_3$@glass and d-f) CsPbBr$_{1.5}$I$_{1.5}$@glass on perovskite concentration. The samples of S$_{1G}$-S$_{9G}$ and S$_{1R}$-S$_{8R}$ were prepared by heat treatment at 500°C/2hr and 550°C/2hr, respectively.
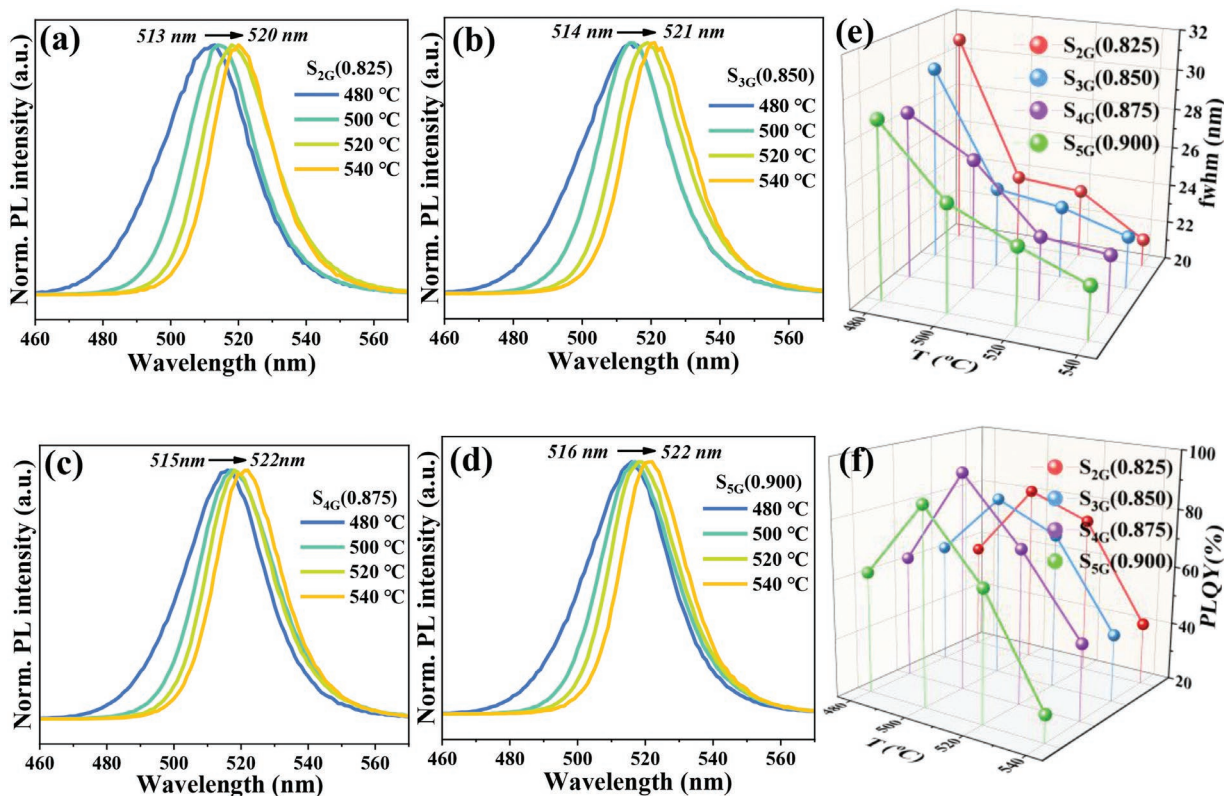

Figure 3. a–d) Normalized PL spectra, e) fwhms and f) PLQYs of S$_{2G}$-S$_{5G}$ samples prepared via different heat-treatment temperatures at 480, 500, 520, and 540°C for 2 hr.
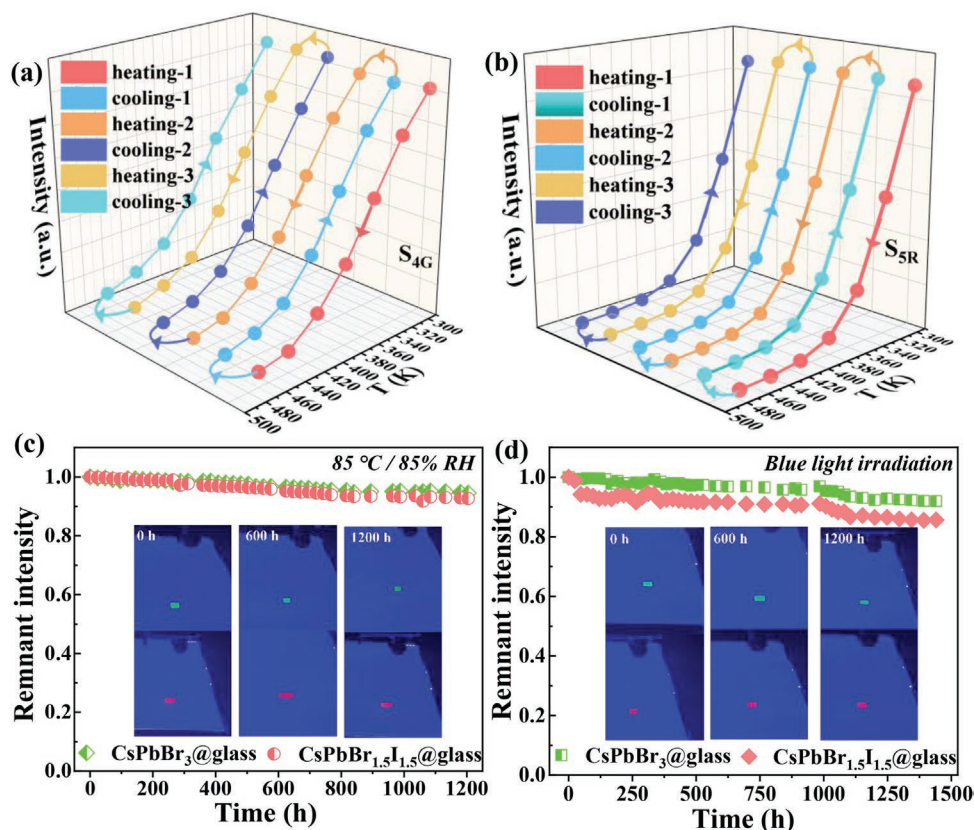
Figure 4. Temperature-dependent PL intensity for a) green CsPbBr$_3$@glass and b) red CsPbBr$_{1.5}$I$_{1.5}$@glass samples experiencing three-time heating/coolibf cycles between 290 K and 470 K. c) Heat/humidity resistance test of CsPbX$_3$@glass under accelerated aging condition at 85 °C/85% RH and d) photostability test under blue light (optical power: 40W m^{-2}) irradiation for 60 days. Insets are illuminated photographs of the corresponding samples after stability tests.

excellent thermal reversibility without observable change in PL intensity after three-time heating/cooling cycles between 290 K and 470 K (Figure 4a,b). Besides, benefited from protection of dense glass network and effective separation of CsPbX$_3$ from external environment, CsPbX$_3$@glass samples also exhibit excellent resistance to humidity and heat (Figure 4c,d). After 1200 h (50 days) of accelerated aging tests (85°C/85% RH), CsPbBr$_3$@glass and CsPbBr$_{1.5}$I$_{1.5}$@glass can maintain 94.5% and 92.6% of the initial PL intensity, respectively (Figure 4c). More importantly, the blue light stability of CsPbX$_3$@glass determines its potential as LCM in blue-light-excited wLED for display application. Therefore, we tested blue-light-irradiation stability by placing CsPbX$_3$@glass on a blue light guide plate with an optical power of 40 W m^{-2}. After 1440 h (60 days) blue light irradiation, CsPbBr$_3$@glass, and CsPbBr$_{1.5}$I$_{1.5}$@glass cam remain 91.9% and 85.6% of their initial PL intensity, respectively (Figure 4d). Finally, mixing CsPbBr$_3$@glass with CsPbBr$_{1.5}$I$_{1.5}$@glass will not lead to halogen-exchange-induced phase separation since both CsPbBr$_3$ and CsPbBr$_{1.5}$I$_{1.5}$ are well separated by glass matrix (Figure S5, Supporting Information).

These excellent optical properties and long-term stability of the green/red CsPbX$_3$@glass (X$_3$ = Br$_3$, Br$_{1.5}$I$_{1.5}$) validate their suitability as LCM in wLEDs for back-lighting display. As a proof-of-concept experiment, LED devices are constructed by coupling green-emitting CsPbBr$_3$@glass powders,

red-emitting CsPbBr$_{1.5}$I$_{1.5}$@glass powders, and the mixture of CsPbBr$_3$@glass and CsPbBr$_{1.5}$I$_{1.5}$@glass powders with 460 nm blue LED chip. The as-prepared LED devices yield extremely bright green, red, and white luminescence at an operating bias of 3 V (insets of **Figure 5**a–c). This voltage is applied on the blue chip, which can be completely absorbed by CsPbBr$_3$@glass LCM (Figure 5a) and CsPbBr$_{1.5}$I$_{1.5}$@glass one (Figure 5b) to produce pure green and red light. When coupling with appropriate amount of CsPbBr$_3$@glass and CsPbBr$_{1.5}$I$_{1.5}$@glass LCMs, the device can produce a combined white light consisting of 460 nm blue (LED chip), 517 nm green (CsPbBr$_3$@glass) and 640 nm red (CsPbBr$_{1.5}$I$_{1.5}$@glass) tri-color narrowband emissions (Figure 5c). By optimizing the ratio of red to green PeQDs@glass powders, red/green/blue tri-color intensities can be finely tuned, and the as-prepared wLED can produce cool, pure, and warm white light (Figure S6, Supporting Information). The device performance of CsPbX$_3$@glass-based LEDs is summarized in Figure 5d–f. The green, red and white LED devices show high external quantum efficiency (EQE) of 15.1%, 8.0%, and 13.8% at low operating currents, respectively, which will gradually decrease with increase of current. The power efficiency for the constructed wLED is 25.8 lm W^{-1}. Fortunately, the LEDs can achieve ultra-high luminance of 600 000 (green), 100 000 (red), and 500 000 cd m^{-2} (white), respectively. Different to the case of EQE, the luminance remains quite high value

**ADVANCED
SCIENCE NEWS**
www.advancedsciencenews.com

**ADVANCED
FUNCTIONAL
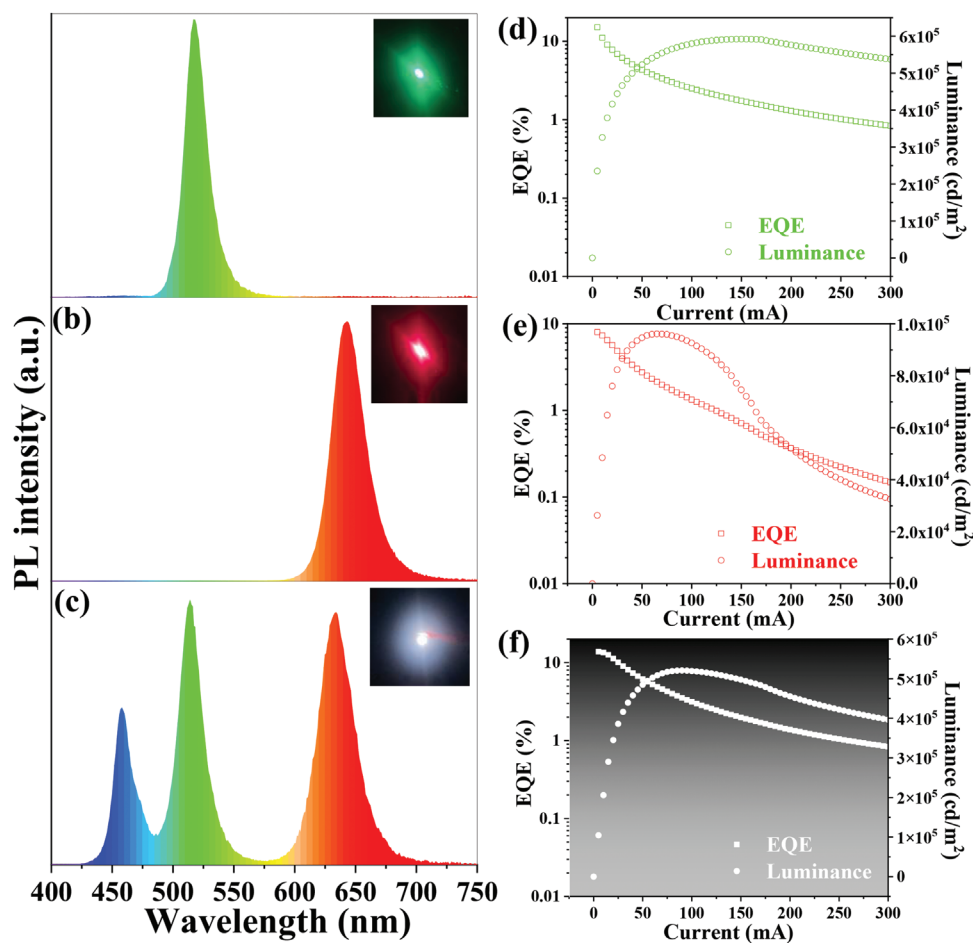MATERIALS**
www.afm-journal.de

Figure 5. a–c) PL spectra for the constructed CsPbX$_3$@glass converted green LED, red LED and white LED. Insets of the corresponding PL photographs of the working LED devices at 3 V. EQE and luminance versus driving current for d) green LED, e) red LED, and f) white LED.

even at high operating currents. For instance, the luminance of wLED still reaches as high as 400 000 cd m^{-2} at a high current of 300 mA, which ensures its practical application in LCD as back-lighting source.

For concept demonstration, we have assembled a back-lighting source by embedding 36 CsPbX$_3$@glass-based wLEDs on the two sides of light guiding plate (LGP) (**Figure 6**a–d). The main function of LGP is to guide the spot white light from wLEDs to the plane white light. Indeed, PL spectrum recorded from LPG shows blue/green/red tri-color narrowband emissions (Figure 6e), and high-brightness and uniform plane white light is clearly observable under the driving voltage/current of 12 V per 2A (Figure 6f). A demo display device was successfully designed by combining a commercial TFT-LCD panel with the present CsPbX$_3$@glass-based wLED arrays in the LGP (Figure 6g; Figure S7, Supporting Information). As demonstrated in Figure 6h, an image with a logo of "Fujian Normal University" and white background is converted via single-chip micyoco and integrated circuit, and finally is displayed in the screen. We detected radiance PL intensities of specifically selected six positions in the LCD screen with the help of a luminance meter. Evidently, blue/green/red tri-color spectral profiles are similar (Figure S8, Supporting Information) and the

radiance intensities are almost the same for all these positions (Figure 6i), confirming color and brightness uniformity of the display device. Furthermore, we directly recorded the brightness value every other day for 9 days and took photos of the display. No obvious variation in radiance and image is found (Figure S9, Supporting Information), evidencing excellent stability for the prototype display device.

Finally, we compare the present prototype LCD device with a commercial LCD (ZT0007, Shenzhen Kaiyixing Electronics Co., LTD) to confirm its wide-color-gamut feature. The backlight source of commercial LCD consists of blue LED chips and YAG: Ce phosphors, which produces a combined white light originated from blue emission of LED and a broadband yellow emission of Ce^{3+}: 4f–4f transition (Figure S10, Supporting Information). The images of two kinds of LCD devices based on the commercial backlit unit and the present CsPbX$_3$@glass backlit unit are presented in **Figure 7**a–d. Compared to traditional YAG:Ce-wLED backlight, the displays adopting CsPbX$_3$@glass-wLED backlight exhibit more details of object colors. For instance, for the display of green color image, the commercial one yields a yellowish green color (Figure 7a), while the CsPbX$_3$@glass-based one presents a pure green color and a more remarkable
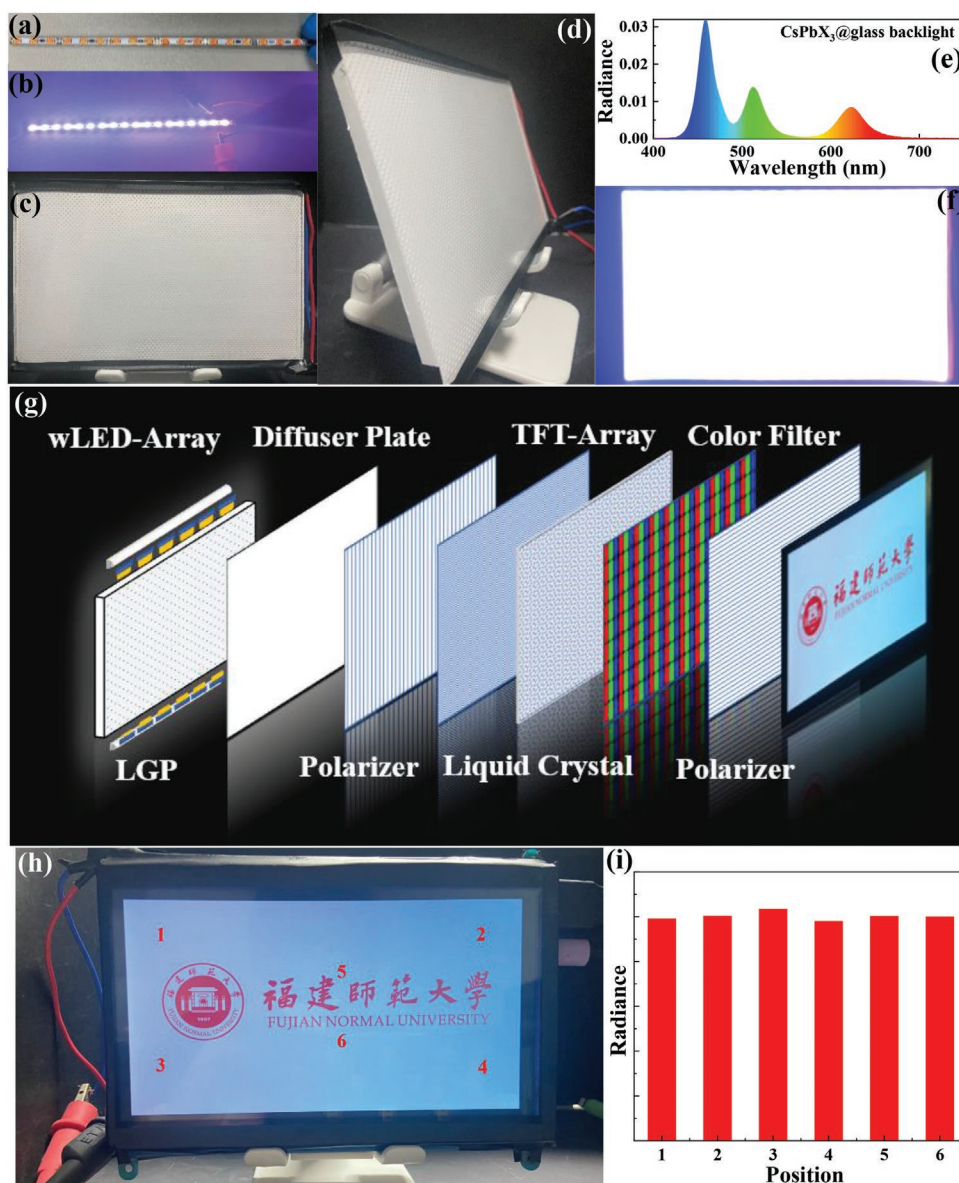
Figure 6. Photographs of a,b) CsPbX$_3$@glass-based wLED array and c,d) LGP coupled with two wLED arrays. e) PL spectrum and f) luminescent photograph of LGP under a operating voltage of 12 V. g) Schematic structure of the CsPbX$_3$@glass-based back-lighting LCD system. h) Photograph of the designed CsPbX3@glass backlit LCD in operation and i) radiance PL intensities from six different detecting positions in LCD screen.

color rendition (Figure 7c). Similarly, display image with a pure red color and a high saturation is easily realized for the CsPbX$_3$@glass-based LCD (Figure 7d). We directly measured radiance PL spectra for the pure white, blue, and green images in the two LCD screens via a luminance meter. The recorded spectra have been filtered by the color filters (Figure S11, Supporting Information) and blue/green/red images show concomitant weak PL bands of other colors besides dominant emissive profiles (Figure 7e). Evidently, the fwhm values for both green and red emissions (26 nm, 33 nm) from the CsPbX$_3$@glass-based LCD are far narrower than those (69 nm, 54 nm) from the commercial one (Figure 7e). As a consequence, according to the calculated CIE color coordinates (Table S7, Supporting Information), the

color gamut of the CsPbX$_3$@glass-based LCD reaches as high as 127% of NTSC standard and 176% of that of the commercial one (Figure 7f).

3. Conclusion

In summary, we have successfully prepared CsPbX$_3$@glass with tunable emitting wavelength, high PLQY, and excellent stability by modulating perovskite concentration in glass and heat-treatment temperature. The best PLQYs of green CsPbBr$_3$@glass and red CsPbBr$_{1.5}$I$_{1.5}$@glass can reach 94% and 78%, respectively, which are the highest values for the CsPbX$_3$ embedded glasses reported so far. Due to the effective protection of robust glass,
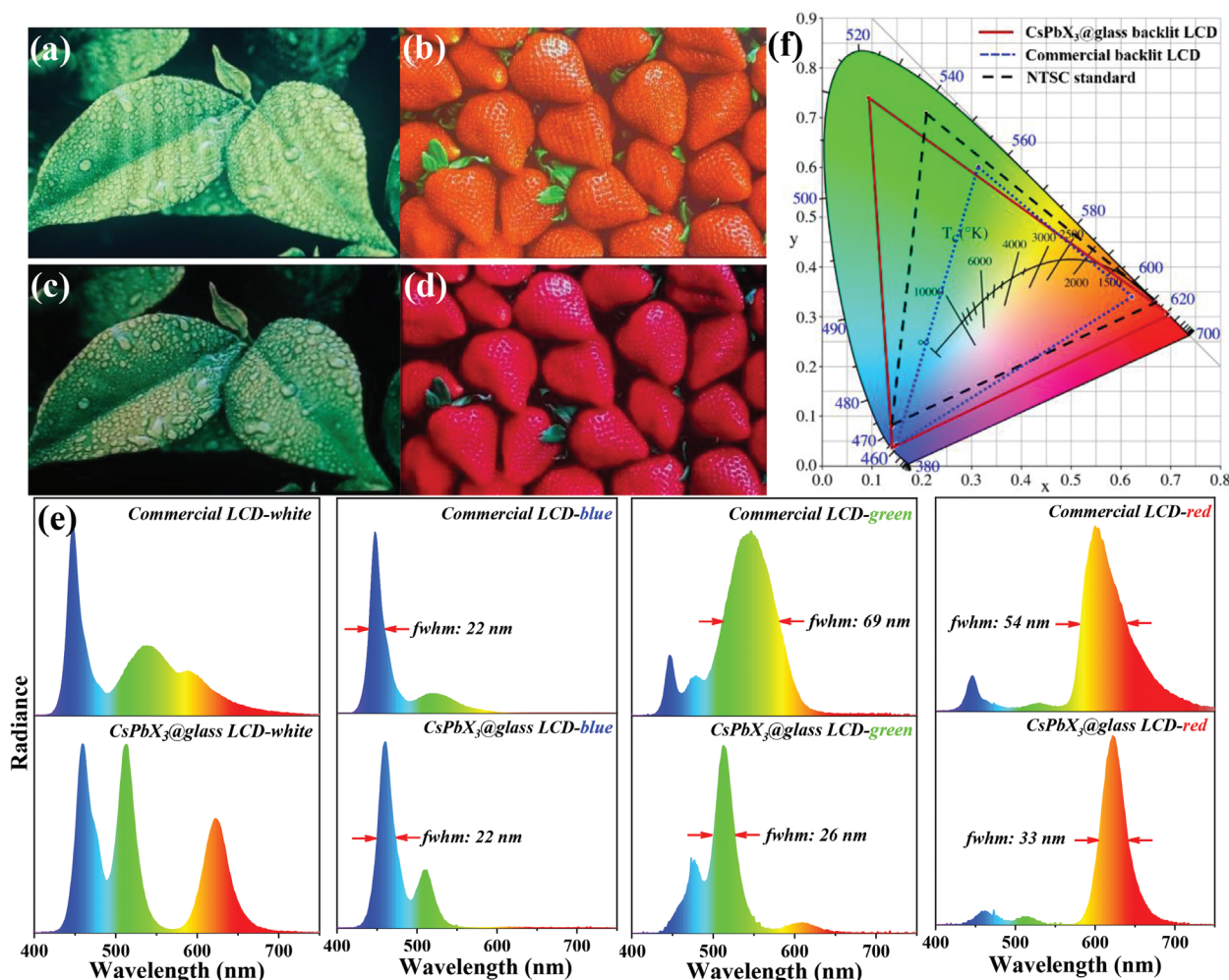
Figure 7. Display images for LCD screens with a,b) commercial YAG: Ce-converted wLED backlit unit and c,d) CsPbX$_3$@glass-based wLED backlit unit. e) PL radiance spectra directly recorded from commercial LCD screen and CsPbX$_3$@glass-based LCD screen via a luminance meter for pure white, blue, green, and red images. f) Color gamut of CsPbX$_3$@glass-based backlit unit (red solid triangle), commercial backlit unit (blue dot triangle) and NSTC 1953 standard (black dash triangle).

CsPbX$_3$ can withstand a variety of harsh stability tests. After 50 days of commercial standard aging at 85 °C/85 %RH, PL intensity of CsPbBr$_3$ and CsPbBr$_{1.5}$I$_{1.5}$ remains 94.5% and 92.6% of initial values, respectively; after 60 days of blue light radiation, the value maintains 91.9% and 85.6% of initial ones, respectively. As an application demo, an elaborately designed brand-new CsPbX$_3$@glass-converted wLED backlight source can produce efficient, stable, and narrowband red/green/blue tri-color emissions, and endow prototype LCD device with more details of object colors and wide color gamut covering 127% of the NTSC 1953 standard and 176% of the commercial LCD. The admirable optical performance and excellent long-term stability of the present CsPbX$_3$@glass demonstrate their promising potential in the application of high-quality backlit display.

Conflict of Interest

The authors declare no conflict of interest.

Data Availability Statement

Research data are not shared.

Supporting Information

Supporting Information is available from the Wiley Online Library or from the author.

[1] J. Y. Kim, O. Voznyy, D. Zhitomirsky, E. H. Sargent, *Adv. Mater.* **2013**, *25*, 4986.

[2] J. Shamsi, A. S. Urban, M. Imran, L. De Trizio, L. Manna, *Chem. Rev.* **2019**, *119*, 3296.

[3] Y. Shu, X. Lin, H. Qin, Z. Hu, Y. Jin, X. Peng, *Angew. Chem., Int. Ed.* **2020**, *59*, 22312.

[4] X. Wang, Z. Bao, Y.-C. Chang, R.-S. Liu, *ACS Energy Lett.* **2020**, *5*, 3374.

[5] L. Protesescu, S. Yakunin, M. I. Bodnarchuk, F. Krieg, R. Caputo, C. H. Hendon, R. X. Yang, A. Walsh, M. V. Kovalenko, *Nano Lett.* **2015**, *15*, 3692.

[6] S. A. Veldhuis, P. P. Boix, N. Yantara, M. Li, T. C. Sum, N. Mathews, S. G. Mhaisalkar, *Adv. Mater.* **2016**, *28*, 6804.

[7] Y. Wang, X. Li, J. Song, L. Xiao, H. Zeng, H. Sun, *Adv. Mater.* **2015**, *27*, 7101.

[8] A. Swarnkar, R. Chulliyil, V. K. Ravi, M. Irfanullah, A. Chowdhury, A. Nag, *Angew. Chem., Int. Ed.* **2015**, *54*, 15424.

[9] F. Liu, Y. Zhang, C. Ding, S. Kobayashi, T. Izuishi, N. Nakazawa, T. Toyoda, T. Ohta, S. Hayase, T. Minemoto, K. Yoshino, S. Dai, Q. Shen, *ACS Nano* **2017**, *11*, 10373.

[10] C. Sun, Z. Gao, Y. Deng, H. Liu, L. Wang, S. Su, P. Li, H. Li, Z. Zhang, W. Bi, *ACS Appl. Mater. Interfaces* **2019**, *11*, 34109.

[11] D. Yu, F. Cao, Y. Gao, Y. Xiong, H. Zeng, *Adv. Funct. Mater.* **2018**, *28*, 1800248.

[12] K. Lin, J. Xing, L. N. Quan, F. P. G. de Arquer, X. Gong, J. Lu, L. Xie, W. Zhao, D. Zhang, C. Yan, W. Li, X. Liu, Y. Lu, J. Kirman, E. H. Sargent, Q. Xiong, Z. Wei, *Nature* **2018**, *562*, 245.

[13] Y. Shen, Y.-Q. Li, K. Zhang, L.-J. Zhang, F.-M. Xie, L. Chen, X.-Y. Cai, Y. Lu, H. Ren, X. Gao, H. Xie, H. Mao, S. Kera, J.-X. Tang, *Adv. Funct. Mater.* **2022**, *32*, 2206574.

[14] J. S. Kim, J.-M. Heo, G.-S. Park, S.-J. Woo, C. Cho, H. J. Yun, D.-H. Kim, J. Park, S.-C. Lee, S.-H. Park, E. Yoon, N. C. Greenham, T.-W. Lee, *Nature* **2022**, *611*, 688.

[15] J. Jiang, Z. Chu, Z. Yin, J. Li, Y. Yang, J. Chen, J. Wu, J. You, X. Zhang, *Adv. Mater.* **2022**, *34*, 2204460.

[16] Z. Chen, Z. Li, Z. Chen, R. Xia, G. Zou, L. Chu, S.-J. Su, J. Peng, H.-L. Yip, Y. Cao, *Joule* **2021**, *5*, 456.

[17] Z. Xia, Q. Liu, *Prog. Mater. Sci.* **2016**, *84*, 59.

[18] R. Zhang, H. Lin, Y. Yu, D. Chen, J. Xu, Y. Wang, *Laser Photonics Rev.* **2014**, *8*, 158.

[19] S. Li, L. Wang, D. Tang, Y. Cho, X. Liu, X. Zhou, L. Lu, L. Zhang, T. Takeda, N. Hirosaki, R.-J. Xie, *Chem. Mater.* **2018**, *30*, 494.

[20] M.-H. Fang, W.-L. Wu, Y. Jin, T. Lesniewski, S. Mahlik, M. Grinberg, M. G. Brik, A. M. Srivastava, C.-Y. Chiang, W. Zhou, D. Jeong, S. H. Kim, G. Leniec, S. M. Kaczmarek, H.-S. Sheu, R.-S. Liu, *Angew. Chem., Int. Ed.* **2018**, *57*, 1797.

[21] M. Zhao, K. Cao, M. Liu, J. Zhang, R. Chen, Q. Zhang, Z. Xia, *Angew. Chem., Int. Ed.* **2020**, *59*, 12938.

[22] J. Lin, Y. Lu, X. Li, F. Huang, C. Yang, M. Liu, N. Jiang, D. Chen, *ACS Energy Lett.* **2021**, *6*, 519.

[23] C. Sun, Y. Zhang, C. Ruan, C. Yin, X. Wang, Y. Wang, W. W. Yu, *Adv. Mater.* **2016**, *28*, 10088.

[24] S. Zou, Y. Liu, J. Li, C. Liu, R. Feng, F. Jiang, Y. Li, J. Song, H. Zeng, M. Hong, X. Chen, *J. Am. Chem. Soc.* **2017**, *139*, 11443.

[25] X. Li, Y. Wang, H. Sun, H. Zeng, *Adv. Mater.* **2017**, *29*, 1701185.

[26] S. Wang, C. Bi, J. Yuan, L. Zhang, J. Tian, *ACS Energy Lett.* **2018**, *3*, 245.

[27] F. Li, S. Huang, X. Liu, Z. Bai, Z. Wang, H. Xie, X. Bai, H. Zhong, *Adv. Funct. Mater.* **2021**, *31*, 2008211.

[28] F. Krieg, S. T. Ochsenbein, S. Yakunin, S. ten Brinck, P. Aellen, A. Süess, B. Clerc, D. Guggisberg, O. Nazarenko, Y. Shynkarenko, S. Kumar, C.-J. Shih, I. Infante, M. V. Kovalenko, *ACS Energy Lett.* **2018**, *3*, 641.

[29] Y. Wei, Z. Cheng, J. Lin, *Chem. Soc. Rev.* **2019**, *48*, 310.

[30] S. Su, J. Tao, C. Sun, D. Xu, H. Zhang, T. Wei, Z.-H. Zhang, Z. Wang, C. Fan, W. Bi, *Chem. Eng. J.* **2021**, *419*, 129612.

[31] J. Han, D. Xu, C. Sun, H. Zhang, T. Wei, J. Tao, C. Fan, W. Bi, *ACS Appl. Energy Mater.* **2022**, *5*, 13461.

[32] S. Yuan, D. Chen, X. Li, J. Zhong, X. Xu, *ACS Appl. Mater. Interfaces* **2018**, *10*, 18918.

[33] B. Ai, C. Liu, J. Wang, J. Xie, J. Han, X. Zhao, *J. Am. Ceram. Soc.* **2016**, *99*, 2875.

[34] R. Yuan, L. Shen, C. Shen, J. Liu, L. Zhou, W. Xiang, X. Liang, *Chem. Commun.* **2018**, *54*, 3395.

[35] M. Xia, J. Luo, C. Chen, H. Liu, J. Tang, *Adv. Opt. Mater.* **2019**, *7*, 1900851.

[36] Y. Ye, W. Zhang, Z. Zhao, J. Wang, C. Liu, Z. Deng, X. Zhao, J. Han, *Adv. Opt. Mater.* **2019**, *7*, 1801663.

[37] X. Huang, Q. Guo, D. Yang, X. Xiao, X. Liu, Z. Xia, F. Fan, J. Qiu, G. Dong, *Nat. Photonics* **2020**, *14*, 82.

[38] K. Sun, D. Tan, X. Fang, X. Xia, D. Lin, J. Song, Y. Lin, Z. Liu, M. Gu, Y. Yue, J. Qiu, *Science* **2022**, *375*, 307.

[39] J. Li, Y. Fan, T. Xuan, H. Zhang, W. Li, C. Hu, J. Zhuang, R.-S. Liu, B. Lei, Y. Liu, X. Zhang, *ACS Appl. Mater. Interfaces* **2022**, *14*, 30029.

[40] Z. Xu, T. Chen, J. Xia, T. Man, G. Zheng, J. Yan, X. Liu, H. Zhang, J. Qiu, *J. Am. Ceram. Soc.* **2022**, *105*, 3303.

[41] Z. Chen, Q. Wang, Y. Tong, X. Liu, J. Zhao, B. Peng, R. Zeng, S. Pan, B. Zou, W. Xiang, *J. Phys. Chem. Lett.* **2022**, *13*, 4701.

[42] Z. Xu, X. Liu, C. Jiang, D. Ma, J. Ren, C. Cheng, J. Qiu, *J. Am. Ceram. Soc.* **2018**, *101*, 1508.

[43] D. Chen, Y. Liu, C. Yang, J. Zhong, S. Zhou, J. Chen, H. Huang, *Nanoscale* **2019**, *11*, 17216.

[44] C. Yang, B. Zhuang, J. Lin, S. Wang, M. Liu, N. Jiang, D. Chen, *Chem. Eng. J.* **2020**, *398*, 125616.

[45] D. Wang, J. Qiu, D. Zhou, S. Hu, Y. Wen, K. Zhang, Q. Wang, Y. Yang, H. Wu, Z. Long, X. Li, J. Pi, E. Cao, *Chem. Eng. J.* **2021**, *421*, 127777.

[46] Z. Yang, H. Zhang, Z. Fang, J. Yi, P. Song, X. Yu, D. Zhou, J. Qiu, X. Xu, *Chem. Eng. J.* **2022**, *427*, 131379.

[47] G. Lakshminarayana, E. M. Weis, B. L. Bennett, A. Labouriau, D. J. Williams, J. G. Duque, M. Sheik-Bahae, M. P. Hehlen, *Opt. Mater.* **2012**, *35*, 117.

[48] R. E. Youngman, M. J. Dejneka, *J. Am. Ceram. Soc.* **2002**, *85*, 1077.

[49] X. Zhang, L. Guo, Y. Zhang, C. Cheng, Y. Cheng, X. Li, J. Zhang, S. Xu, Y. Cao, J. Sun, L. Cheng, B. Chen, *J. Am. Ceram. Soc.* **2020**, *103*, 5028.